AALBORG UNIVERSITY
DENMARK

Model Predictive Voltage and Power Control of Islanded PV-Battery Microgrids with Washout Filter Based Power Sharing Strategy

Shan, Y.; Hu, J.; Liu, M.; Zhu, J.; Guerrero, J. M.

Model Predictive Voltage and Power Control of Islanded PV-Battery Microgrids with Washout Filter Based Power Sharing Strategy

[1]Yinghao Shan, *Student Member, IEEE*, Jiefeng Hu, *Senior Member*, *IEEE,* Ming Liu, Jianguo Zhu, *Senior Member*, *IEEE,* and Josep Guerrero, *Fellow*, *IEEE*

Abstract—This paper proposes a new control strategy of microgrids for improved voltage quality. In the existing control techniques, the droop control is commonly adopted as a decentralized power sharing method at the cost of voltage deviations. Besides, the conventional cascaded control featuring relatively slow dynamic response shows difficulties in handling the fluctuation of renewable energy outputs, leading to further voltage quality deterioration. In this paper, an advanced model predictive power control strategy by considering the battery constraints is proposed for bidirectional dc-dc converters to smooth the solar photovoltaic (PV) outputs and stabilize the dc-bus voltages. A model predictive voltage control scheme taking into account the voltage changing trend is then developed to control the distributed inverters to improve the output ac voltages. Furthermore, a washout filter based power sharing approach with the plug-and-play capability is adopted to achieve a proper load sharing among parallel inverters and mitigate the voltage deviation. The proposed control strategy is numerically simulated in MATLAB/Simulink and experimentally verified by hardware-in-the-loop (HIL) tests under the condition of fluctuating PV outputs and variable power demands. (This paper is accompanied by a video showing the HIL test.)

Index Terms--Model predictive control, islanded microgrid, dc power source, washout filter, power sharing

I. INTRODUCTION

Microgrids integrated with distributed generators (DGs), such as solar photovoltaics (PVs), wind turbines, fuel cells and energy storages, are widely recognized as a promising solution for future power grids with high reliability and power quality [1]. By the bus types, microgrids can be categorized into ac, dc, and hybrid bus types. Owing to the fact that the vast existing loads are supplied by the ac power, a major task of microgrids is still to supply high-quality ac power [2]. As the electronic interface between the power sources and the loads, the power converters play an important role in microgrids. For this reason, the development of high-performance control strategies for

these power converters has attracted increasing interests [3].

Unlike the grid-connected microgrids that are strongly supported by the stiff utility grid, it is vital to share the load power properly while maintaining stable voltage and frequency for an islanded microgrid. Conventionally, the droop control method is used for power sharing [4]-[6]. However, it presents several drawbacks, such as the tradeoff between the voltage regulation and the power sharing accuracy [7], [8], poor power quality with nonlinear loads [9], and low precision of power sharing with mixed resistive and inductive transmission lines [10].

To eliminate the voltage and frequency deviations caused by the droop control method, the secondary control can be employed [4, 11-15]. A central based secondary control using the PID regulator is presented in [4] to restore the frequency and voltage at the point of common coupling (PCC). Note that, in this study, the PCC is defined as the terminals of every DG (including its transmission line to the ac bus), or the nearest common point of the parallel system that can be connected to the utility grid, as shown in Fig.1 (here the switch is OFF). A fuzzy-secondary-controller is proposed in [11] to regulate the voltage and frequency. However, the centralized secondary control suffers from the inherent properties of communication technology, such as delay and data loss. On the other hand, the distributed secondary control approaches with reduced communication burden have drawn much attention. For example, a distributed finite-time secondary control is proposed in [12] for both voltage and frequency restoration. A multi-functional distributed secondary control with a voltage regulator, a reactive power regulator, and an active power/frequency regulator is presented in [13]. In [14], a washout filter-based power sharing method is proposed, which is capable of regulating the voltage and frequency to the rated values. For the islanded microgrids, the equivalence between the distributed secondary control and the washout filter-based power sharing method is demonstrated in [15]. The washout filter based method has shown a promising potential to share the power and restore the voltage and frequency simultaneously. However, the incapacity of the washout filter to restore the PCC voltage to the rated value is overlooked in [14,15], and the "equivalence" has also its limitation. Therefore, the washout filter based method is still under development and needs to be further explored in distributed power systems.

Despite all the research efforts to improve the performance of droop control for microgrids, no major change has been achieved in the inner control structure, in which the conventional cascaded linear control has been applied for decades. The use of such cascaded linear control at the bottom

Y. Shan, J. Hu and M. Liu are with the Department of Electrical Engineering, The Hong Kong Polytechnic University, Hung Hom, Hong Kong (e-mail: yh.shan@connect.polyu.hk; jerry.hu@polyu.edu.hk; leo.m.liu@connect.polyu.hk).
J. Zhu is with the School of Electrical and Information Engineering, University of Sydney, Sydney, Australia (e-mail: jianguo.zhu@sydney.edu.au)
J. M. Guerrero is with the Department of Energy Technology, Aalborg University, Aalborg DK-9220, Denmark (e-mail: joz@et.aau.dk)
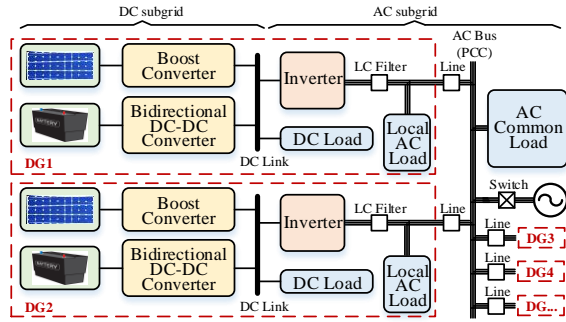
Fig. 1. A microgrid with PV energy sources and multiple converters.

Fig. 2. DC-side circuitry and the control diagram of the proposed MPPC.

can significantly deteriorate the effectiveness of higher-level control in the hierarchical control structure. This is unfortunately neglected by many researchers [16,17]. The main problem is that, in practice, fluctuating output from renewables can cause oscillations in the dc-bus voltage, which in turn, deteriorates the power quality on the ac side. The traditional cascaded control featuring relatively slow dynamics is not effective to deal with these fluctuations.

In contrast to the cascaded linear control, the model predictive control (MPC) is based on the minimization of a predefined cost function by studying the predicted response of a power converter over a finite time duration at each time step. Due to its fast dynamics and flexible control scheme in which different constraints can be readily formulated, MPC has been widely used for the control of power converters. Examples include MPC of dc-ac converters for islanded systems [18]-[20], ac-dc converters to absorb grid power and accommodate dc loads [21,22], bidirectional dc-dc converters [23], dc-dc boost converters [24], and dc-dc buck converters [25]. While these techniques have been applied in electric drives and individual DGs, they do not address large systems with multiple power converters. In microgrids with renewable energy sources and various kinds of loads, new challenges facing the researchers include the intermittency of renewable energy sources, load sharing, and power quality, etc., which are still open issues for MPC.

Inspired by the abovementioned problems, this paper proposes a new control scheme for microgrids with practical renewable energy resources, energy storage and local loads to supply reliable and high-quality power. Fig.1 shows the topology of such a microgrid with PV energy sources and multiple converters. A model predictive power control (MPPC) is developed to control the bidirectional dc-dc converter of the battery energy storage system (BESS) in the dc subgrid, while a model predictive voltage control (MPVC) combined with a washout filter based power sharing method is proposed to control the parallel voltage source inverters (VSIs). The contributions in this study are highlighted as follows:

1) Instead of using a constant power supply as the VSI dc input, a PV-battery system is used by considering the practical renewable power generation and energy storage. An improved MPPC method is developed to deal with the fluctuating power generation from PVs and to maintain a stable dc-bus voltage. It requires only the measurements inside the BESS.

2) The washout filter based control method is adopted to perform power sharing. Compared to the droop control method, the washout filter based power sharing method does not need any communication lines either, while having the capability to improve the voltage and frequ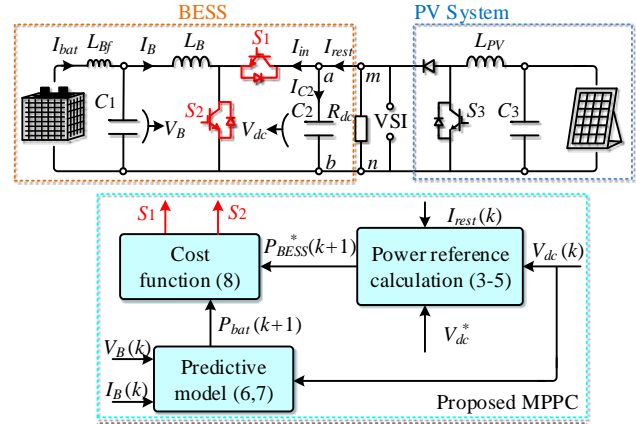ency regulation, and compensate the voltage and frequency deviations. The limitation of the "equivalence" in [15] and the incapacity of washout filter to restore the PCC voltage to the rated value are analyzed. The corresponding solution is proposed to further compensate the PCC voltage.

3) An MPVC strategy is used to replace the cascaded linear control loops. To our best knowledge, it is the first time to incorporate the washout filter based method with MPC method, and the performance is compared with that using the cascaded linear control. In addition, the MPVC strategy considers the changing trend of the voltage trajectory aimed at perfecting the tracking processes so as to further improve the voltage quality.

This paper is organized as follows. Section II presents the MPPC for the dc power control. Section III describes the washout filter based power sharing method. Section IV presents the MPVC and its improved cost function, followed by the overall control strategy. The numerical simulation and experimental hardware-in-the-loop (HIL) tests are respectively presented in Sections V and VI. Conclusions are drawn in Section VII.

II. MPPC OF BIDIRECTIONAL BUCK-BOOST CONVERTERS

In the PV system shown in Fig.2, a dc-dc boost converter with maximum power point tracking (MPPT) capability is used. The incremental conductance and integral regulator techniques are applied in the MPPT controller for fast and efficient tracking [26], which will not be discussed here as it is not the main focus of this work.

Each BESS unit consists of a battery and a bidirectional buck-boost converter. In an islanded microgrid, the aim of BESS is to bridge the gap of power between the renewable energy sources and the load demand. Since the power supplied/absorbed by the BESS is controlled by the buck-boost converter, it is necessary to obtain the effect of its switching states on the power supplied/absorbed. From the detailed circuit of the BESS and its connection to the rest of system shown in Fig.2, by applying the Kirchoff's current law, the currents flowing in and out of Node a can be expressed as

$$I_{in} = I_{rest} - I_{C2} \tag{1}$$

where I_{in} denotes the current absorbed by BESS, I_{rest} the current flowing into Node a (i.e. the current from the rest of microgrid), and I_{C2} the current flowing through the dc-bus capacitor C_2.

Since the power balance can be indicated by a stable dc-bus voltage, the required power to be supplied/absorbed by the

BESS to keep the power balance within the microgrid can be calculated by

$$P_{BESS}^* = \left| I_{in} \cdot V_{dc}^* \right| \tag{2}$$

where V_{dc}^* is the reference voltage of dc bus.

According to the principle outlined in [27], at the k-th sampling instant, the current flowing through C_2 can be predicted by

$$I_{C2}(k+1) = \frac{1}{N}\left(\frac{C_2}{T_s}(V_{dc}^* - V_{dc}(k))\right) \tag{3}$$

where N is the coefficient, T_s the sampling time, and V_{dc} the actual dc-bus voltage. Please note that N here is not strictly equal to an integer value, which is differentiated from [23,28].

Accordingly, I_{in} can be predicted by

$$I_{in}(k+1) = I_{rest}(k) - I_{C2}(k+1) \tag{4}$$

As a result, the required power to be supplied/absorbed by the BESS can be predicted as

$$P_{BESS}^*(k+1) = \left| I_{in}(k+1) \cdot V_{dc}^* \right| \tag{5}$$

The discrete-time model of the bidirectional buck-boost converter can be expressed as

$$\begin{cases} S_2 = 0, S_1 = 1 : I_B(k+1) = \dfrac{T_s}{L_B}(-V_{dc}(k) + V_B(k)) + I_B(k) \\ \\ S_2 = 1, S_1 = 0 : I_B(k+1) = \dfrac{T_s}{L_B}V_B(k) + I_B(k) \end{cases} \tag{6}$$

where 0 and 1 indicate the switching OFF and ON states; V_B and I_B are the battery voltage and inductor current, respectively; and the current flowing out of the battery is defined as positive.

The battery output power can then be predicted as

$$P_{bat}(k+1) = \left| I_B(k+1) \cdot V_B(k) \right| \tag{7}$$

Through the bidirectional buck-boost converter, the power balance can be guaranteed by minimizing the following cost function

$$J_P = \left(P_{BESS}^*(k+1) - P_{bat}(k+1) \right)^2 \tag{8}$$

$$s.t.\ SOC_{\min} \le SOC \le SOC_{\max},\ P_{bat} \le P_{bat\_rated}$$

The proposed MPPC approach is illustrated by the block diagram in Fig.2. At the k-th time instant, the rest of the current outside the BESS, $I_{rest}(k)$, the actual dc-link voltage, $V_{dc}(k)$, and the dc-link voltage reference, V_{dc}^*, are used to calculate the required BESS power at the $(k+1)$th instant, $P_{BESS}^*(k+1)$, according to (3)-(5). Meanwhile, $V_B(k)$ and $I_B(k)$, together with $V_{dc}(k)$, will be used to predict $I_B(k+1)$. The predicted battery output power, $P_{bat}(k+1)$, is then obtained according to (6) and (7). Finally, the switching state that can minimize the cost function (8) will be selected to control the buck-boost converter.

It is noted that this procedure requires only the measurements inside BESS, whereas the method proposed in [28] requires additional measurement of the PV output current. The use of additional current sensors and communications will increase the system cost and deteriorate the system reliability, particularly in power networks with high PV penetration. Therefore, the proposed MPPC strategy for BESS shows a useful improvement over the one in [28].

III. THE WASHOUT FILTER BASED POWER SHARING STRATEGY

A. Droop Power Sharing Method

After the PV output is smoothed and the dc-bus voltage is maintained by the BESS, we can now proceed to control the ac subgrid of the microgrid. To coordinate the power sharing among the distributed power sources, the famous droop control method, which mimics the behavior of a synchronous generator, is conventionally adopted without critical communication. It can be expressed as [4, 29]

$$f = f^* - mP \tag{9}$$

$$E = E^* - nQ \tag{10}$$

where f and f^* are the measured and reference frequency values, E and E^* the measured and reference voltage values, m and n the droop coefficients, and P and Q the actual dispatched active and reactive powers, respectively.

By using the droop control method, frequency and voltage deviations are inevitable due to the droop characteristics expressed in (9) and (10).

In order to address the abovementioned issue, a secondary control method is commonly adopted. For both frequency and voltage, the errors between their rated and actual values are delivered to the proportional-integral (PI) controllers to generate the required compensations. This secondary control principle in the s-domain can be expressed as [30]

$$f_c = k_{pf}(f^* - f) + \frac{k_{if}}{s}(f^* - f) \tag{11}$$

$$E_c = k_{pE}(E^* - E) + \frac{k_{iE}}{s}(E^* - E) \tag{12}$$

where f_c and E_c are the frequency and voltage compensations, k_{pf}, k_{if}, k_{pE}, and k_{iE} the PI coefficients for frequency and voltage compensation, respectively.

In this scenario, a central controller with low bandwidth communication lines are needed. Such centralized secondary control suffers from the inherent properties of communication technology, such as delay and data loss. These problems can be mitigated by introducing the washout filter based power sharing strategy.

B. Conditioned Equivalence of Washout Filter Based Method and Secondary Control Method

The washout filter based power sharing strategy can be derived by combining the droop and secondary control methods, as outlined below [15].

Taking frequency, f, as an example, we can rewrite the droop control method with the secondary control's compensation as

$$f = f^* - mP + f_c \tag{13}$$

By considering only the integration ($k_{pf}=0$), (11) can be simplified as

$$f_c = \frac{k_{if}}{s}(f^* - f) \tag{14}$$

Substituting (13) into (14) yields

$$f_c = \frac{k_{if}}{s}(f^* - (f^* - mP + f_c)) = \frac{k_{if}}{s}(mP - f_c) \tag{15}$$

Therefore,

$$f_c = \frac{k_{if}}{s + k_{if}}mP \tag{16}$$
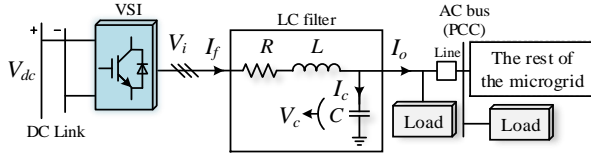
Substituting (16) in (13), one obtains

Fig. 3. AC-side circuitry.

$$f = f^* - \frac{s}{s+k_{if}} mP \tag{17}$$

Compared to (9), (17) contains an extra component $s/(s+k_{if})$. This is exactly the transfer function of a typical washout filter. The washout filter is a high-pass filter [31]. It can block the dc component and pass the transient component, which makes the power sharing more robust against parameter uncertainties [32]. In the same way, (10) can be correspondingly changed to

$$E = E^* - \frac{s}{s+k_{iE}} nQ \tag{18}$$

From this point of view, the washout filter based power sharing strategy described by (17) and (18) is endowed with the capability to restore the frequency and voltage gaps caused by the droop control method while the communication-free and decentralized features can be kept. This equivalence is nevertheless conditioned by the following restrictions:

1) The frequency and voltage are measured locally in the controller, not from the PCC, which is different from the central based secondary control.

2) The frequency and voltage that can be restored to the rated values are the controlled frequency and voltage, i.e f and V in (17) and (18), respectively.

3) The target voltage which is aimed to be restored is the filter capacitor's voltage of the inverter, i.e. the inverter output voltage. This voltage can be restored to the rated value under the no load condition. However, when a high-power local load is connected, the restoration will be deteriorated.

These restrictions limit the effect of the washout filter serving as the secondary controller to eliminate the deviations. This limitation will be analyzed, and a solution will be given in the section below.

C. Improved Washout Filter with PCC Voltage Compensation

In a microgrid, the frequency is a global quantity, independent of where it is measured or changed. If using the droop control method, according to (9), the changing active power will affect the instantaneous frequency everywhere in the system. However, the situation is different when it comes to the voltage. Due to the existing impedance of transmission lines, the voltage will drop across these lines, leading to an unequal sharing of reactive power. According to (10), this kind of reactive power sharing reversely causes the voltage drops complicatedly. The voltage drop across the transmission line impedance can be approximately calculated by [33]

$$eE \approx \frac{XQ_e + RP_e}{E^*} \tag{19}$$

where eE is the voltage drop across the impedance, X and R are the inductive and resistive components of the impedance, Q_e and P_e the reactive and active powers passing through the impedance, respectively, and E^* is the reference voltage value.

Equation (19) shows that although the washout filter method can restore the inverter output voltage to the rated value, the PCC voltage will still drop due to the transmission line

impedance. This PCC voltage drop will bring more challenges to the grid-connection process.

In order to further compensate the deviation and recover the voltage dip, eE can be used with an added coefficient, dv. Thus, the final voltage control will be

$$E = E^* - \frac{s}{s+k_{iE}} nQ + dv \cdot eE \cdot \underbrace{\frac{f_l}{s+f_l}}_{lowpass\ filter} \tag{20}$$

One concern is how to obtain the information of the transmission line impedance, i.e. X and R, since they are not always readily available. Currently, the developed offline and online methods can help solve this problem. The offline method uses the original systematic states to evaluate the impedance [34]. While the online method utilizes the real-time measurements to estimate the impedance [35]. Since this is out of the scope of this study, the transmission line impedance here can be treated as an available parameter.

Another concern is how to determine the value of dv. This can be achieved by using the energy management system (EMS), which is always necessary for a power-electronic-based microgrid [4]. EMS also provides the values of Q_e and P_e which are either measured or calculated. Since the adjustment of dv can raise the inverter output voltage, it must follow the local electric power supply rules. In this study, the voltage threshold φ is 10%. This threshold defines the upper approximation of dv as the following

$$dv \le \varphi \cdot E^* \Big/ \left(\frac{XQ_0 + RP_0}{E^*} \right) \tag{21}$$

where Q_0 and P_0 are related to the DG's capacity. Inside this interval, we can adjust dv to flexibly raise the PCC voltage in a certain range. Thus, the further compensated PCC voltage will reduce the risk for grid connection. In addition, this proposed method can effectively avoid the breakdown of the whole system caused by the failure of a single unit from the central secondary control.

IV. MPVC OF DC-AC INVERTERS

Once the voltage reference generated from the washout filter for power sharing is obtained, the next task is to control the inverters. The control can be implemented in the $\alpha\beta$ stationary orthogonal reference frame rather than the abc reference frame due to the advantage of less computation. The variable x (voltage or current) in the $\alpha\beta$ frame can be obtained by the Clarke transformation as

$$x_{\alpha\beta} = \frac{2}{3}[1 \ e^{(2\pi/3)j} \ e^{(4\pi/3)j}][x_a \ x_b \ x_c]^T = x_\alpha + jx_\beta \tag{22}$$

A. The Conventional MPVC Method

The two-level three-phase VSI is the most common inverter used in microgrids to provide ac power supplies. In total, a VSI generates eight (2^3) feasible switching states expressed as

$$\begin{cases} i = 1,2,...,6 : V_i = \frac{2}{3} V_{dc} e^{(i-1)(\pi/3)j} \\ i = 0,7 : V_i = \mathbf{0} \end{cases} \tag{23}$$

Accordingly, the gating signal combination $(S_a \ S_b \ S_c)$ are 000, 100, 110, 010, 011, 001, 101, and 111, respectively. Fig.3 shows the configuration of ac subgrid.

As shown in Fig.3, a VSI is attached with an LC filter, which is used to mitigate the harmonics and supply sinusoidal voltage to the ac loads, where R is the resistance, L the inductance, and

C the capacitance of the LC filter, respectively.

To analyze the capacitor dynamics, one can obtain

$$C\frac{dV_c}{dt} = I_C = I_f - I_o \qquad (24)$$

where V_c and I_c are the capacitor voltage and current, and I_f and I_o the inductor and output currents, respectively.

According to the Kirchoff's voltage law, one obtains

$$L\frac{dI_f}{dt} = V_i - I_f R - V_c \qquad (25)$$

Combining (24) and (25), one obtains a state-space model as [18], [20]

$$\frac{d\boldsymbol{x}}{dt} = \boldsymbol{A}\boldsymbol{x} + \boldsymbol{B}\boldsymbol{y} \qquad (26)$$

where

$$\boldsymbol{x} = \begin{bmatrix} V_c \\ I_f \end{bmatrix}, \quad \boldsymbol{y} = \begin{bmatrix} V_i \\ I_o \end{bmatrix}, \quad \boldsymbol{A} = \begin{bmatrix} 0 & 1/C \\ -1/L & -R/L \end{bmatrix}, \quad \boldsymbol{B} = \begin{bmatrix} 0 & -1/C \\ 1/L & 0 \end{bmatrix}$$

Accordingly, the following discrete-time model can be derived

$$\boldsymbol{x}(k+1) = e^{T_s A}\boldsymbol{x}(k) + A^{-1}(e^{T_s A} - \boldsymbol{I}_{2\times2})\boldsymbol{B}\boldsymbol{y}(k) \qquad (27)$$

where $\boldsymbol{I}_{2\times2}$ is the identity matrix. By using (27), the capacitor voltage at the $(k+1)$th instant can be predicted. Conventionally, in order to provide a stable voltage supply, the cost function considering the voltage amplitude is formulated as

$$J_V = \left(V_{c\alpha}^* - V_{c\alpha}(k+1)\right)^2 + \left(V_{c\beta}^* - V_{c\beta}(k+1)\right)^2 \qquad (28)$$

where $V_{c\alpha}(k+1)$ and $V_{c\beta}(k+1)$ are the real and imaginary parts of the predicted capacitor voltage, and $V_{c\alpha}^*$ and $V_{c\beta}^*$ the real and imaginary parts of the reference voltage, respectively. The voltage vector with its corresponding gating signal that can minimize the cost function of (28) will be selected and generated by the VSI.

B. The Improved MPVC with Voltage Quality Enhancement

From the conventional design point of view, the cost function J_V only considers the amplitude of the objective voltage. This is unlikely to be able to guarantee a tight amplitude tracking since the objective voltage is always prone to change with time, and the vibrations around the reference trajectory are more likely to occur. This deteriorates the tracking accuracy.

To solve this problem, this paper adopts an improved tracking method which can take into account the trend of change such that the objective voltage trajectory can be tightly fixed [36]. Fig.4 illustrates the main idea. At the k-th time instant, assuming both the conventional and improved tracking methods have an identical amplitude error, ΔE_0, to the reference and present the same trend of change with respect to the reference (i.e. the slopes of trajectories, S_{con0} and S_{imp0}, equal S_{ref0}). For the sake of simplicity, only two alternative predicted values, V_1 and V_2, are discussed, i.e. V_1 or V_2 will be selected in the future decision at the next step prediction horizon. At the $(k+1)$th instant as shown in Fig.4, V_1 and V_2 have the same error, ΔE_1, to the reference trajectory, the conventional and improved tracking methods can either pass through V_1 or V_2. In this case, just considering the voltage amplitude is not helpful, but once the slope is also included in the determination, the trajectory of improved track is more likely to be obtained with $S_{imp1} = S_{ref1}$. Otherwise, the
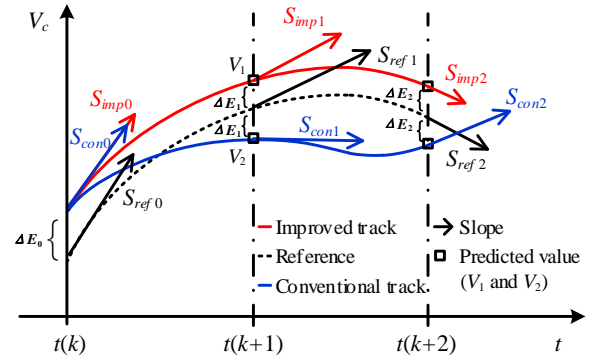

Fig. 4. Voltage tracking analysis.

conventional track may happen when $S_{con1} \neq S_{ref1}$, resulting in an inferior track.

This situation may deteriorate as the $(k+2)$th time instant is considered for one step delay compensation. Under the same error, ΔE_2, when the slope is respected ($S_{imp2} = S_{ref2}$), the improved tracking method can tightly follow the reference. Otherwise, when the slope is overlooked ($S_{con2} \neq S_{ref2}$), the tracking trajectory by the conventional method will deflect the reference, leading to a higher harmonic distortion. In short, if the slope (i.e. the trend of change) is also considered in the determination (i.e. the cost function), the tracking trajectory (i.e. the improved track) will approach the reference as closely as possible.

The slope can be obtained by calculating the derivative of the capacitor voltage. In order to introduce the derivative terms into the cost function, it should consist of two parts, the referenced and the predicted derivative values of the inverter output voltage (i.e. the capacitor voltage V_c).

To get the referenced derivative value, we start with the expression of the capacitor voltage reference, that is

$$\begin{aligned} V_c^* &= V_{c\alpha}^* + jV_{c\beta}^* \\ &= V_c \sin(\omega t(k)) + jV_c \cos(\omega t(k)) \end{aligned} \qquad (29)$$

where ω is the angular frequency.

Taking derivatives of (29) yields

$$\begin{aligned} \frac{dV_c^*}{dt} &= \omega V_c \cos(\omega t(k)) - j\omega V_c \sin(\omega t(k)) \\ &= \omega V_{c\beta}^* - j\omega V_{c\alpha}^* \end{aligned} \qquad (30)$$

The predicted derivative value of V_c based on the discrete-time model of (24) can then be calculated as

$$\begin{aligned} \frac{dV_c(k+1)}{dt} &= \frac{I_f(k+1) - I_o(k)}{C} \\ &= \frac{I_{f\alpha}(k+1) - I_{o\alpha}(k)}{C} + j\frac{I_{f\beta}(k+1) - I_{o\beta}(k)}{C} \end{aligned} \qquad (31)$$

where $I_{f\alpha}(k+1)$ and $I_{f\beta}(k+1)$ are obtained from (27).

To minimize both the real and imaginary tracking errors between the references of (30) and the predicted values of (31), the following cost function can be formulated

$$J_{VD} = \left(\omega V_{c\beta}^* - (\frac{i_{f\alpha}(k+1) - i_{o\alpha}(k)}{C}) \right)^2 + \left(\omega V_{c\alpha}^* + (\frac{i_{f\beta}(k+1) - i_{o\beta}(k)}{C}) \right)^2 \qquad (32)$$

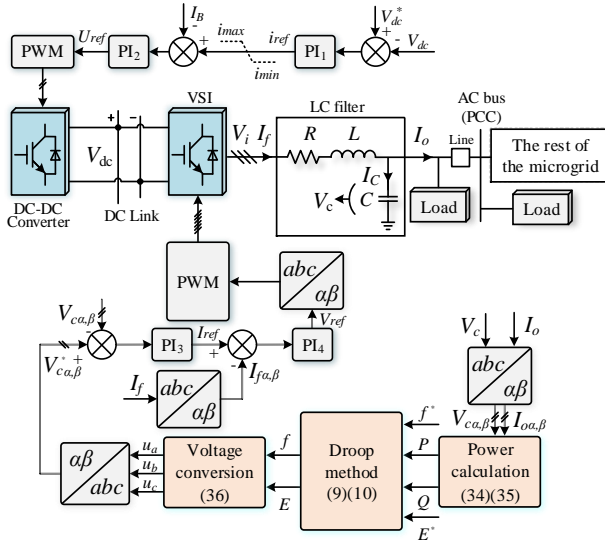Finally, the complete improved cost function is

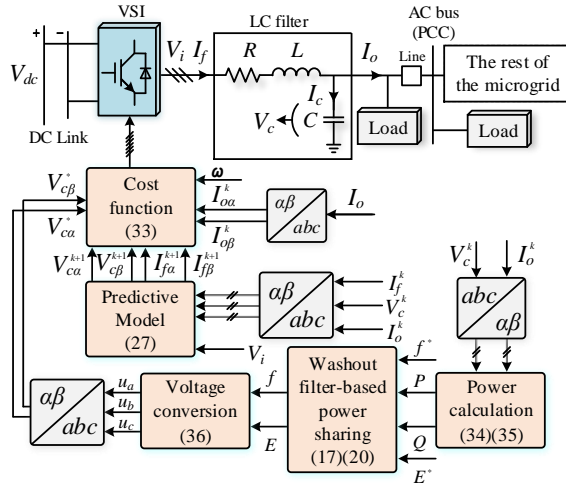Fig. 5. Block diagram of the conventional overall control scheme.

Fig. 6. Proposed overall control strategy of inverters (improved MPVC & improved washout filter based power sharing strategy).

$$J = aJ_V + bJ_{VD} \tag{33}$$

where *a* and *b* are the weighting coefficients. The first term is used to track the voltage amplitude, and the second term to track the voltage changing trend. This cost function will be used to evaluate each possible voltage vector. The optimal switching state that minimizes *J* is selected and applied to control the inverter.

C. Overall Control Strategy

For better comparison, the conventional droop method with cascaded inner feedback loops and the proposed overall control strategy are depicted in Fig.5 and Fig.6, respectively. For the proposed strategy, firstly, *P* and *Q* are calculated by

$$P = \frac{3}{2}(V_{c\alpha}I_{o\alpha} + V_{c\beta}I_{o\beta}) \cdot \underbrace{\frac{f_l}{s + f_l}}_{\text{lowpass filter}} \tag{34}$$

$$Q = \frac{3}{2}(V_{c\beta}I_{o\alpha} - V_{c\alpha}I_{o\beta}) \cdot \underbrace{\frac{f_l}{s + f_l}}_{\text{lowpass filter}} \tag{35}$$

where f_l is the cut-off frequency of the lowpass filter.

Next, the washout filter-based power sharing method will generate the frequency and voltage references. A three-phase voltage conversion is then required to transform this frequency and voltage into three-phase sinusoidal voltages through
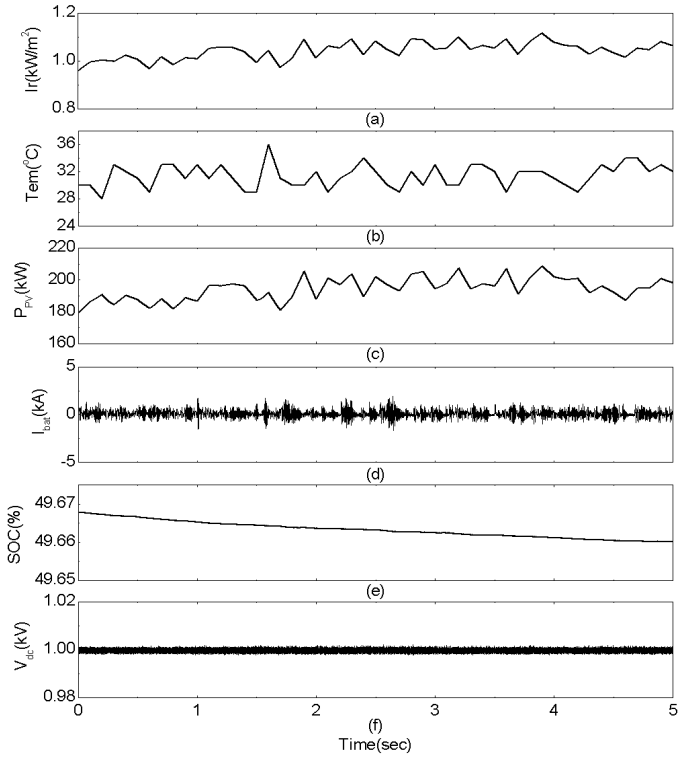

Fig. 7. Performance of the proposed MPPC method. The waveforms from top to bottom are (a) solar irradiation, (b) ambient temperature, (c) PV output power, (d) battery current, (e) battery SOC, (f) dc-bus voltage.

$$\begin{cases} u_a = E\sin(2\pi f + 0) \\ u_b = E\sin(2\pi f - 2\pi/3) \\ u_c = E\sin(2\pi f + 2\pi/3) \end{cases} \tag{36}$$

where u_a, u_b, and u_c are the three phase voltages. These voltage references will then be delivered to the inner MPVC controller.

V. NUMERICAL SIMULATION

In this section, the microgrid shown in Fig.1 and the proposed control strategies illustrated in Figs.2 and 6 are numerically simulated by using MATLAB/Simulink. Table I lists the system parameters. The settings for both DG1 and DG2 are the same. A diode-bridge rectifier with a capacitor and a resistor in parallel is used as a nonlinear load. The system starts operating with the initial dc and ac loads as listed in Table I, and then, follows a sequence of events containing the load changes as described in Table II.

TABLE I. System Parameters

| Description	Value
Solar PV	SunPower Spr-305-WHT, 200kW (STD)
Battery	Lithium-Ion, 500V, 1.6kA·h
DC rated voltage	1000V
DC-side circuit	$L_{Bf} = 50\mu H$, $L_B = 170\mu H$, $L_B = 80mH$, $C_1 = 50mF$, $C_2 = 26mF$, $C_3 = 100\mu F$
AC-bus voltage	380V (p-p, rms), 50Hz
AC-bus LC filter	$R = 0.02\Omega$, $L = 3.6mH$, $C = 200\mu F$
Line impedance	$R_{line} = 0.1\Omega$, $L_{line} = 2.4mH$
MPPC	$N = 1$
Power sharing	$m = 1.25e\text{-}5$, $n = 8.33e\text{-}5$, $k_{if} = 15$, $k_{iE} = 10$, $f_l = 6.25Hz$
Washout filter	$dv = 1.84$ during 1s ~ 3s, other time: 1.62
MPVC	Improved:($a = 0.8$, $b = 0.2$), Conventional:($a = 1$, $b = 0$)
Sampling interval	20µs
Initial dc loads	DG1: 20kW, DG2: 20kW
Initial ac loads	DG1: (50kW, 0kVar), DG2: (50kW, 0kVar)
AC common load	(40kW, 10kVar)
Nonlinear ac load	$R_{nl} = 75\Omega$, $C_{nl} = 20mF$
Double loops	PI$_1$: ($k_p = 10$, $k_i = 50$), PI$_2$: ($k_p = 1.5$, $k_i = 1$); PI$_3$: ($k_p = 5$, $k_i = 0.2$), PI$_4$: ($k_p = 0.24$, $k_i = 0.01$)
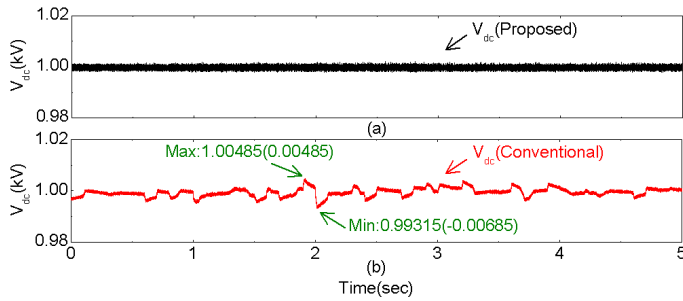
Fig. 8. Comparison of dc-bus voltages (a) proposed MPPC method, (b) conventional cascaded control with double loops.
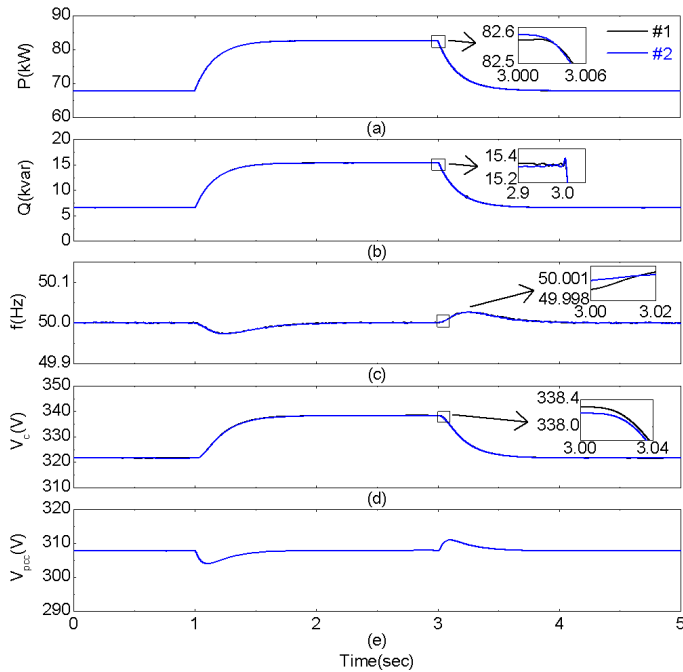

Fig. 9. Overall performance of the proposed washout filter and improved MPVC strategy of Inverter#1 and #2. The waveforms from top to bottom are (a) active power, (b) reactive power, (c) frequency, (f) inverter output voltage, (g) PCC voltage.

TABLE II. Events

Event	Operations	Time(s)
1	AC common load increases from (40kW, 10kVar) to (80kW, 20kVar)	1s
2	Each DG's dc load increases from 20kW to 40kW	2s
3	AC common load decreases from (80kW, 20kVar) to (40kW, 10kVar)	3s

A. MPPC of BESS in DC Subgrid

Fig.7 presents the performance of the proposed MPPC scheme under fluctuating solar irradiation and ambient temperature profiles. The variable load demands follow the events in Table II. As shown in Fig.7(c), a varying PV output power is generated due to the fluctuating solar irradiation and ambient temperature. By using the proposed MPPC strategy, a stable and smooth dc-link voltage can be maintained, as shown in Fig.7(f). Fig.7(d) shows the charging and discharging currents of the battery, while the corresponding state of charge (SOC) of the battery is shown in Fig. 7(e).

Under the same condition of power generation and consumption, Fig.8 compares the dc-link voltages by using the proposed MPPC scheme and the conventional method of double loops to control the bidirectional buck-boost converter. As
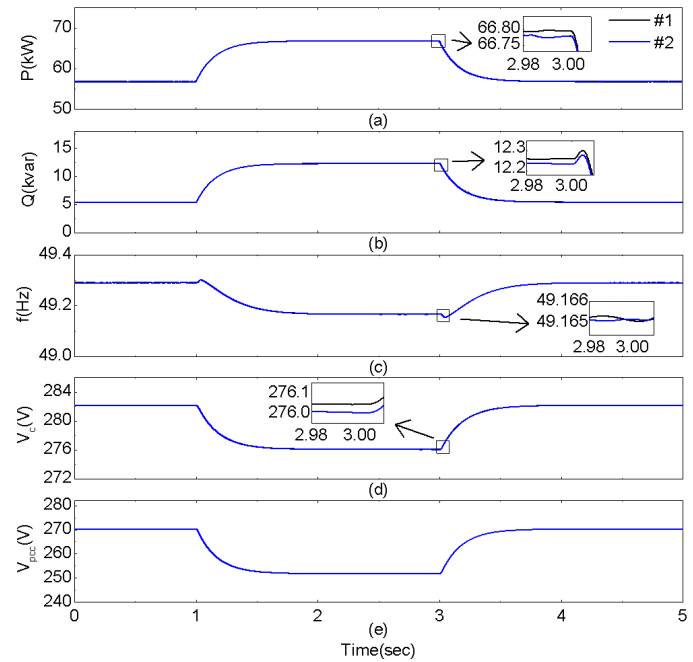

Fig. 10. Overal performance of the conventional droop method with cascaded double feedback loops of Inverter#1 and #2. The waveforms from top to bottom are (a) active power, (b) reactive power, (c) frequency, (f) inverter output voltage, (g) PCC voltage.
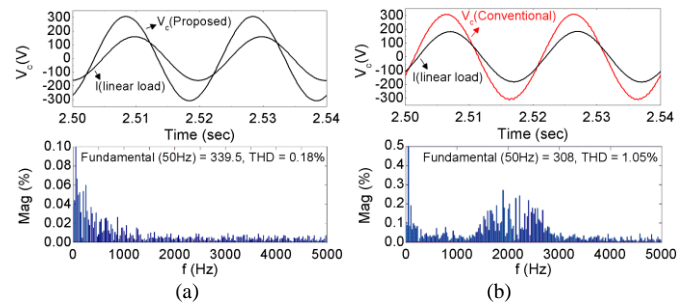

Fig. 11. Comparison of voltage quality under linear load (a) washout filter power sharing strategy with improved MPVC scheme, and (b) washout filter power sharing strategy with conventional MPVC scheme.
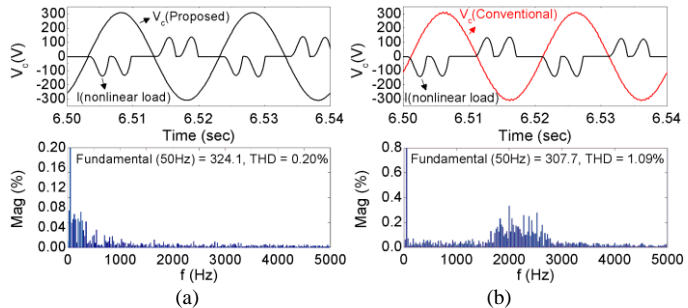

Fig. 12. Comparison of voltage quality under nonlinear load (a) washout filter power sharing strategy with improved MPVC scheme, (b) washout filter power sharing strategy with conventional MPVC scheme.

shown in Fig.8(b), from the nominal value 1 kV, the maximum positive deviation is 0.00485 (+0.485%), while the maximum negative deviation is -0.00685 (-0.685%). Comparing Fig.8(a) and Fig.8(b), it is clearly observed that by using the MPPC scheme, the variable PV outputs can be smoothed and the dc-bus voltage can be maintained more effectively. This is a very encouraging finding because it can not only supply a high-quality dc voltage for dc loads, but also can provide a stable dc source for the inverter.

TABLE III. Events of a microgrid with four DGs

Event	Operations	Time(s)
1	AC common load increases from (60kW, 10kVar) to (120kW, 20kVar)	1s
2	AC common load decreases from (120kW, 20kVar) to (60kW, 10kVar)	3s
3	DG4 is cut out suddenly	5s
4	DG4 is cut in suddenly	7s

TABLE IV. Voltage and frequency deviations

Methods	PCC voltage deviation (ΔV)	Frequency deviation (ΔHz)
Conventional droop & cascaded control	-58.5080	-0.8330
Improved washout filter & improved MPVC	-2.4411	-0.0033
ΔV=Actual PCC voltage – nominal voltage		
ΔHz=Actual frequency – nominal frequency		

B. MPVC and Washout Filter Based Power Sharing Strategy in AC Subgrid and Expansion to More DGs

After the PV outputs have been smoothed and dc-bus voltages can be maintained in the dc subgrid, the performance of the ac subgrid will be evaluated. As listed in Table I, the high-power local load (50 kW) is connected to each DG to evaluate the performance of the proposed washout filter based power sharing strategy with the improved MPVC scheme. Fig.9 shows the results under the same condition of power generation and consumption. It can be seen that inverter #1 and #2 can adjust its output accordingly when the loads vary. Meanwhile, the frequency and the PCC voltage can be restored to the nominal level. In contrast, by using the conventional droop power sharing approach combined with the conventional cascaded linear inverter control method, both the frequency and voltage show more obvious deviations, which deteriorates the power quality, as presented in Figs.10(c) and (e).

The voltage tracking capability of the improved MPVC algorithm is further demonstrated in Fig.11 with the zoom-in voltage waveforms and harmonic analysis. As shown, the voltage under the improved MPVC strategy is more sinusoidal (only 0.18% THD) than that under the conventional MPVC (1.05% THD). Fig.12 shows the performance when feeding a non-linear load consisting of a diode-bridge rectifier with a capacitor and a resistor in parallel. Again, the improved MPVC shows superior performance over the conventional MPVC.

In order not to lose the generality, a microgrid with four DGs is also investigated here to test the effectiveness of the proposed strategy. On the dc side, each DG supplies a 20 kW dc load locally under the same fluctuating solar irradiation and ambient temperature. While on the ac side, the four DGs follow the events in Table III.

As shown in Figs. 13(a) and (b), the four inverters can share the loads equally with no control interconnections. At 5s, DG4 is cut out suddenly while the rest of DGs can pick up the load demand smoothly and accurately. At 7s, when DG4 is connected back into the microgrid, the power sharing returns to the original ratio with only small transient variations. Fig.13(c) depicts the changing trajectory of the systematic frequency. The frequency can be restored to the nominal value no matter what changes in Table III. The inverter output voltage is shown in Fig. 13(d). Fig. 13(e) shows that with the PCC voltage
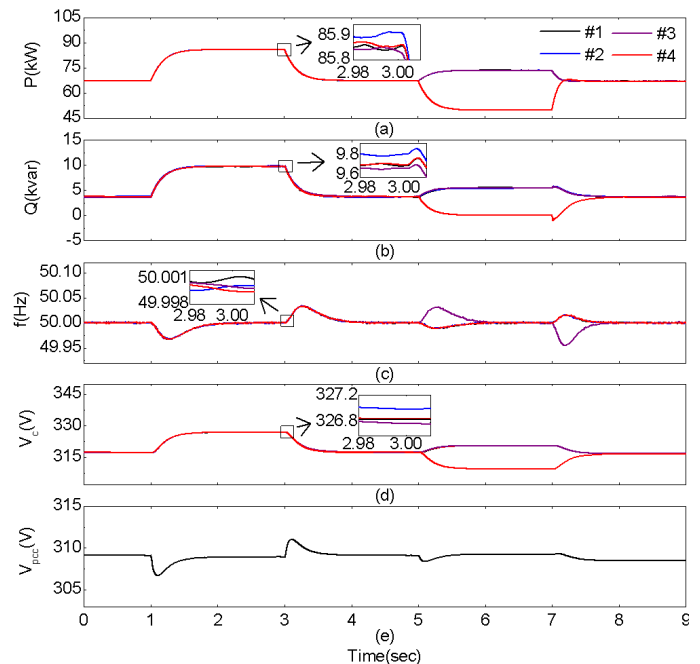

Fig. 13. Performance of the proposed washout filter and MPVC strategy of Inverter#1, #2, #3 and #4. The waveforms from top to bottom are (a) active power, (b) reactive power, (c) frequency, (d) output voltage using washout filter method with PCC voltage compensation, (e) PCC voltage using washout filter method with PCC voltage compensation.
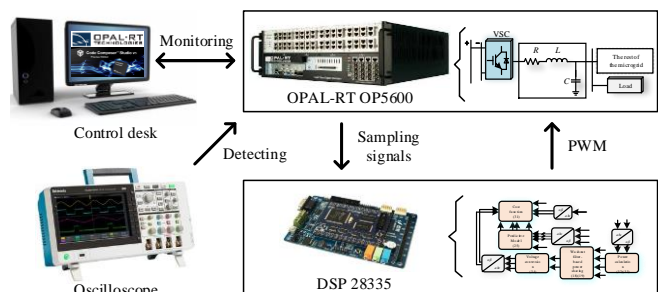

Fig. 14. HIL experimental setup.

compensation, the PCC voltage can be maintained. Moreover, the plug-and-play capability of the proposed strategy is also validated here.

C. Quantitative Comparison of different methods

For a better comparison, the PCC voltage and frequency deviations in Fig. 9 and Fig. 10 at 2s are listed in Table IV. This aims to obtain a quantitative improvement of the proposed overall control over the conventional overall control.

It can be seen that, by using the conventional overall control (i.e., conventional droop & cascaded control), the PCC voltage drops by 58.5080V and the frequency drops by 0.8330Hz after the load changes. On the other hand, by using the proposed overall control (i.e., improved washout filter & improved MPVC), the PCC voltage deviation and frequency deviation have been mitigated significantly to only 2.4411V and 0.0033Hz. This demonstrates the effective voltage and frequency restoration capability of the proposed control strategy.

VI. EXPERIMENTAL HIL TESTS

The proposed control strategy is verified experimentally on an HIL platform, as shown in Fig.14. The control desk delivers the control commends and monitors the microgrid status. The
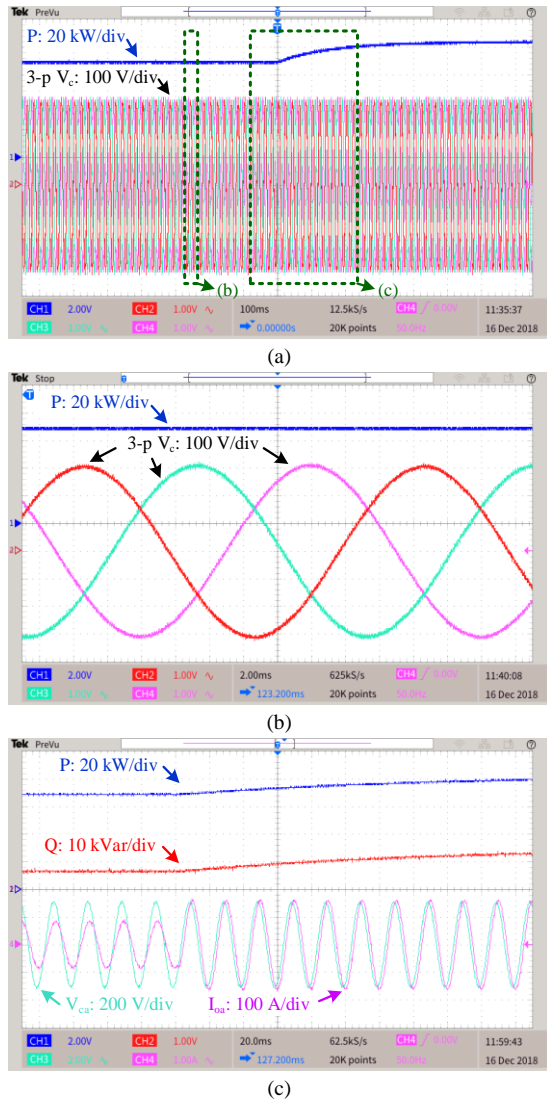
(a)

(b)

(c)

Fig. 15. Performance of the proposed method when ac common load is increased from (40kW, 10kVar) to (80kW, 20kVar). (a) active power and three-phase ac voltages. (b) zoom-in waveforms of active power and three-phase voltages before load changes (c) zoom-in waveforms of active power, reactive power, phase-A voltage and phase-A current during load change transient.

microgrid including the PVs, batteries, power converters and load is implemented in a real-time OPAL-RT simulator, while the control algorithms are programmed in the DSP controller. The DSP controller receives the voltages and currents of the microgrid from the OPAL-RT simulator and then generates the PWM signals to control the power converters. The real-time results can be measured and presented on an oscilloscope via the Analog Output pins from the OPAL-RT simulator.

The effectiveness of the complete proposed method is tested, and the performance of the ac side of the microgrid is presented. Fig.15 shows the microgrid performance during the transient of Event 1 when the ac common load increases from (40 kW, 10 kVar) to (80 kW, 20 kVar). As shown, proper power sharing is achieved while stable high quality voltages are maintained. On the other hand, Fig.16 shows the microgrid performance during the transient of Event 3 when the ac common load decreases from (80 kW, 20 kVar) to (40 kW, 10 kVar). In both cases, the microgrid reaches the steady state in a smooth and safe manner
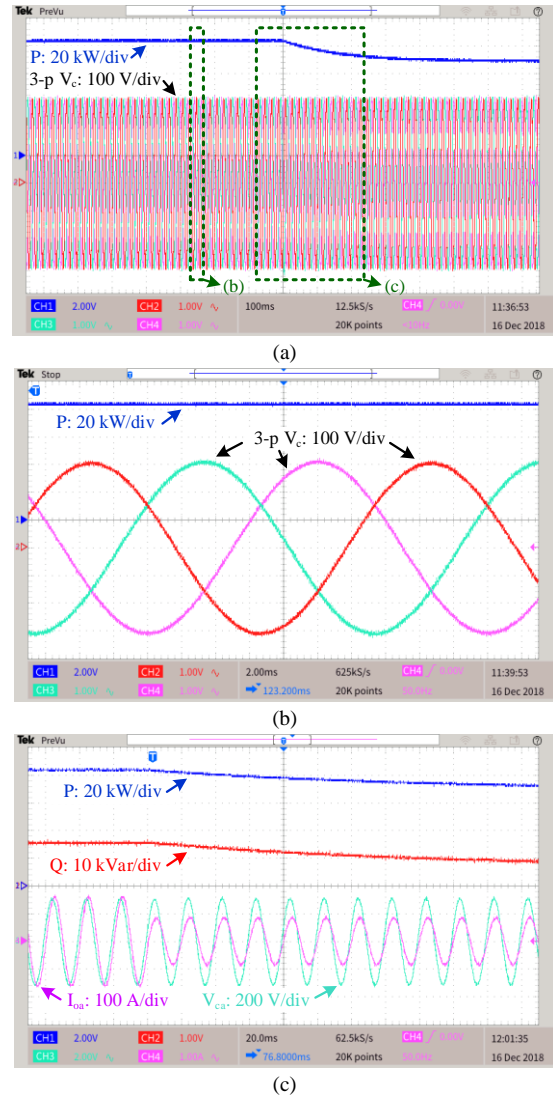

(a)

(b)

(c)

Fig. 16. Performance of the proposed method when ac common load is decreased from (80kW, 20kVar) to (40kW, 10kVar). (a) active power and three-phase ac voltages. (b) zoom-in waveforms of active power and three-phase voltages before load changes (c) zoom-in waveforms of active power, reactive power, phase-A voltage and phase-A current during load change transient.
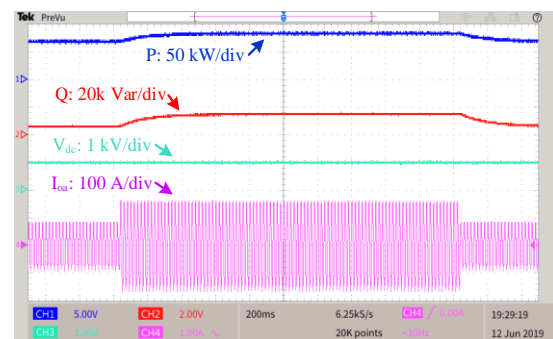

Fig. 17. Overall results of the proposed method when ac common load increases and decreases.

with proper power sharing and stable power supply. Again, since inverter #2 presents similar performance to that of inverter #1, its results are not presented here. It can be seen from Fig.17, the dc-bus voltage keeps stable using proposed method when ac common load changes.
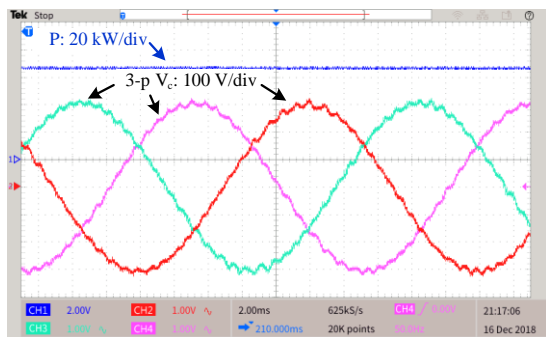
Fig. 18. Performance of the conventional MPVC method & washout filter based power sharing strategy with ac common load at (40kW, 10kVar).

To demonstrate the effectiveness of the improved MPVC scheme separately, the HIL test by using the conventional MPVC with the washout filter based power sharing strategy is conducted, and the results are shown in Fig.18. By comparing Figs.15(b) and 18, it can be observed that the output voltage under the conventional MPVC is distorted with obvious oscillations, especially around voltage peaks. On the other hand, the results of the improved MPVC show a very clean and sinusoidal voltage output because of its excellent voltage tracking capability by considering the voltage changing trend, i.e. by including the voltage derivative constraint in the cost function, as explained in Section IV(*B*).

VII. CONCLUSIONS

In this paper, a microgrid consisting of various distributed power sources and multiple converters with the consideration of the fluctuating renewable energy output and load demand is studied. Based on this, a new control method, essentially integrated of an MPPC scheme for the bidirectional dc-dc converters, an MPVC scheme for the inverters, and a washout filter based power sharing strategy, is proposed. Specifically, the MPPC algorithm aims to effectively smooth the PV output and maintain a stable dc-bus voltage on the dc side of the microgrid. In the ac subgrid, a washout filter based power sharing strategy with the plug-and-play capability is adopted to enable proper load sharing among the distributed inverters according to their power ratings, while the voltage and frequency deviations can be mitigated. An MPVC method is developed to further enhance the ac voltage quality with reduced THD under both linear and nonlinear loads. In comparison with the conventional method, the proposed method presents an overall improvement, showing promising potentials in practical microgrids with intermittent renewables and loads.

REFERENCES

[1] J. Huang, C. Jiang, R. Xu, "A review on distributed energy resources and MicroGrid", *Renew. Sustain. Energy Rev.*, vol. 12, no. 9, pp. 2472-2483, Dec.2008.

[2] P. Yang, Y. Xia, M. Yu, W. Wei, and Y. Peng, "A Decentralized Coordination Control Method for Parallel Bidirectional Power Converters in a Hybrid AC–DC Microgrid," *IEEE Trans. Ind. Electron.,* vol. 65, no. 8, pp. 6217-6228, Aug. 2018.

[3] K. Dai, P. Liu, G. Wang, S. Duan, and J. Chen, "Practical approaches and novel control schemes for a three-phase three-wire series-parallel compensated universal power quality conditioner," *The 19th Annual IEEE Applied Power Electronics Conference and Exposition*, 2004 (APEC04), Anaheim, CA, USA, 2004, Vol.1, pp. 601-606

[4] J. M. Guerrero, J. C. Vasquez, J. Matas, L. G. de Vicuna and M. Castilla, "Hierarchical Control of Droop-Controlled AC and DC Microgrids—A General Approach Toward Standardization," *IEEE Trans. Ind. Electron.*, vol. 58, no. 1, pp. 158-172, Jan. 2011.

[5] X. Li, L. Guo, S. Zhang, C. Wang, Y. Li, A. Chen, Y. Feng, "Observer-Based DC Voltage Droop and Current Feed-Forward Control of a DC Microgrid," *IEEE Trans. Smart Grid*, vol. 9, no. 5, pp. 5207-5216, Sep. 2018.

[6] Y. Sun, X. Hou, J. Yang, H. Han, M. Su and J. M. Guerrero, "New Perspectives on Droop Control in AC Microgrid," *IEEE Trans. Ind. Electron.*, vol. 64, no. 7, pp. 5741-5745, Jul. 2017.

[7] Y. Deng, Y. Tao, G. Chen, G. Li and X. He, "Enhanced Power Flow Control for Grid-Connected Droop-Controlled Inverters with Improved Stability," *IEEE Trans. Ind. Electron.*, vol. 64, no. 7, pp. 5919-5929, Jul. 2017.

[8] B. John, A. Ghosh and F. Zare, "Load Sharing in Medium Voltage Islanded Microgrids With Advanced Angle Droop Control," *IEEE Trans. Smart Grid*, vol. 9, no. 6, pp. 6461-6469, Nov. 2018.

[9] A. Micallef, M. Apap, C. S. Staines, J. M. Guerrero, and J. C. Vasquez, "Reactive power sharing and voltage harmonic distortion compensation of droop controlled single phase islanded microgrids," *IEEE Trans. Smart Grid*, vol. 5, no. 3, pp. 1149-1158, May 2014.

[10] Y. Guan, J. M. Guerrero, X. Zhao, J. C. Vasquez and X. Guo, "A New Way of Controlling Parallel-Connected Inverters by Using Synchronous-Reference-Frame Virtual Impedance Loop—Part I: Control Principle," *IEEE Trans. Power Electron.*, vol. 31, no. 6, pp. 4576-4593, Jun. 2016.

[11] C. Andalib-Bin-Karim, X. Liang and H. Zhang, "Fuzzy-Secondary-Controller-Based Virtual Synchronous Generator Control Scheme for Interfacing Inverters of Renewable Distributed Generation in Microgrids," *IEEE Trans. Ind. Appl.*, vol. 54, no. 2, pp. 1047-1061, Mar.-Apr. 2018.

[12] N. M. Dehkordi, N. Sadati and M. Hamzeh, "Distributed Robust Finite-Time Secondary Voltage and Frequency Control of Islanded Microgrids," *IEEE Trans. Power Syst.*, vol. 32, no. 5, pp. 3648-3659, Sep. 2017.

[13] Q. Shafiee, V. Nasirian, J. C. Vasquez, J. M. Guerrero and A. Davoudi, "A Multi-Functional Fully Distributed Control Framework for AC Microgrids," *IEEE Trans. Smart Grid*, vol. 9, no. 4, pp. 3247-3258, Jul. 2018.

[14] M. Yazdanian and A. Mehrizi-Sani, "Washout Filter-Based Power Sharing," *IEEE Trans. Smart Grid*, vol. 7, no. 2, pp. 967-968, Mar. 2016.

[15] Y. Han, H. Li, L. Xu, X. Zhao and J. M. Guerrero, "Analysis of Washout Filter-Based Power Sharing Strategy—An Equivalent Secondary Controller for Islanded Microgrid Without LBC Lines," *IEEE Trans. Smart Grid*, vol. 9, no. 5, pp. 4061-4076, Sep. 2018.

[16] G. Li, D. Wu, J. Hu, Y. Li, M. S. Hossain, and A. Ghoneim, "HELOS: Heterogeneous load scheduling for electric vehicle-integrated microgrids," *IEEE Trans. Vehicular Technology*, vol. 66, no. 7, pp. 5785–5796, Jul. 2017.

[17] J. Hu, Z. Li, J. Zhu and J. M. Guerrero, "Voltage stabilization: a critical step toward high photovoltaic penetration," *IEEE Ind. Electron. Mag.*, vol. 13, no. 2, pp. 17-30, 2019.

[18] P. Cortes, G. Ortiz, J. I. Yuz, J. Rodriguez, S. Vazquez and L. G. Franquelo, "Model Predictive Control of an Inverter with Output LC Filter for UPS Applications," *IEEE Trans. Ind. Electron.*, vol. 56, no. 6, pp. 1875-1883, Jun. 2009.

[19] M. Preindl and S. Bolognani, "Model predictive direct speed control with finite control set of PMSM drive systems," *IEEE Trans. Power Electron.,* vol. 28, no. 2, pp. 1007-1015, Feb. 2013

[20] J. Hu, Y. Xu, K. W. Cheng and J. M. Guerrero, "A model predictive control strategy of pv-battery microgrid under variable power generations and load conditions," *Appl. Energy*, vol. 221, pp. 195-203, 2018.

[21] Y. Zhang, Z. Li, W. Xu, J. Hu, and J. Zhu, "Grid synchronization of dfig using model predictive direct power control," *in Proc. of International Conf. on Electrical Machines and Systems.*, 2011, 1-6.

[22] J. Hu and K. W. E. Cheng, "Predictive control of power electronics converters in renewable energy systems," *Energies.*, vol. 10, no. 4, pp. 1-14, 2017.

[23] Y. Shan, J. Hu, Z. Li, and J. M. Guerrero, "A Model Predictive Control for Renewable Energy Based AC Microgrids without Any PID Regulators," *IEEE Trans. Power Electron.*, vol. 33, no. 11, pp. 9122-9126, Nov. 2018.

[24] S. El Islam Remache and K. Barra, "Performance comparison among boost and multi level boost converters for photovoltaic grid connected system using finite set model predictive control," *The 9th International Renewable Energy Congress (IREC)*, Hammamet, 2018, pp. 1-6.

[25] Z. Liu, L. Xie, A. Bemporad and S. Lu, "Fast Linear Parameter Varying Model Predictive Control of Buck DC-DC Converters Based on FPGA," *IEEE Access*, vol. 6, pp. 52434-52446, 2018.

[26] M. A. G. de Brito, L. P. Sampaio, G. Luigi, G. A. e Melo, and C. A. Canesin, "Comparative analysis of MPPT techniques for PV applications", *Proc. of Int. Conf. on Clean Elect. Power (ICCEP)*, pp. 99-104, Jun. 2011.

[27] D. E. Quevedo, R. P. Aguilera, M. A. Perez, P. Cortes and R. Lizana, "Model Predictive Control of an AFE Rectifier With Dynamic References," *IEEE Trans. Power Electron.*, vol. 27, no. 7, pp. 3128-3136, Jul. 2012.

[28] Y. Shan, J. Hu, K. W. Chan, Q. Fu and J. M. Guerrero, "Model Predictive Control of Bidirectional DC-DC Converters and AC/DC Interlinking Converters - A New Control Method for PV-Wind-Battery Microgrids," *IEEE Trans. Sustain. Energy*, 2018.

[29] Y. Han, H. Li, P. Shen, E. A. A. Coelho and J. M. Guerrero, "Review of Active and Reactive Power Sharing Strategies in Hierarchical Controlled Microgrids," *IEEE Trans. Power Electron.*, vol. 32, no. 3, pp. 2427-2451, Mar. 2017.

[30] Q. Shafiee, J. M. Guerrero and J. C. Vasquez, "Distributed Secondary Control for Islanded Microgrids—A Novel Approach," *IEEE Trans. Power Electron.*, vol. 29, no. 2, pp. 1018-1031, Feb. 2014.

[31] J. M. Guerrero, J. Matas, V. de, L. G., M. Castilla, and J. Miret, "Wireless-Control Strategy for Parallel Operation of Distributed-Generation Inverters," *IEEE Trans. Ind. Electron.*, vol. 53, no. 5, pp. 1461-1470, Oct. 2006.

[32] M. A. Hassouneh, Hsien-Chiarn Lee and E. H. Abed, "Washout filters in feedback control: benefits, limitations and extensions," in *Proc. of American Control Conference*, Boston, MA, USA, 2004, pp. 3950-3955 vol.5.

[33] J. He and Y. W. Li, "An Enhanced Microgrid Load Demand Sharing Strategy," *IEEE Trans. Power Electron.*, vol. 27, no. 9, pp. 3984-3995, Sep. 2012.

[34] H. Mahmood, D. Michaelson and J. Jiang, "Accurate Reactive Power Sharing in an Islanded Microgrid Using Adaptive Virtual Impedances," *IEEE Trans. Power Electron.*, vol. 30, no. 3, pp. 1605-1617, Mar. 2015.

[35] D. Ritzmann, P. S. Wright, W. Holderbaum and B. Potter, "A Method for Accurate Transmission Line Impedance Parameter Estimation," *IEEE Trans. Instrum. Meas.*, vol. 65, no. 10, pp. 2204-2213, Oct. 2016.

[36] T. Dragičević, "Model Predictive Control of Power Converters for Robust and Fast Operation of AC Microgrids," *IEEE Trans. Power Electron.*, vol. 33, no. 7, pp. 6304-6317, Jul. 2018.